Direct Power Control of Doubly Fed Induction Generator Using Extended Power Theory Under Unbalanced Network

Yongchang Zhang, *Senior Member, IEEE*, Jian Jiao, and Donglin Xu

***Abstract*—This paper proposes a novel direct power control (DPC) method for the doubly fed induction generators (DFIGs) power control system. The proposed DPC method is based on extended power theory rather than conventional instantaneous power theory. The proposed method calculates the rotor reference voltage based on the principle of deadbeat power control. Then, it synthesizes the rotor reference voltage using space vector modulation (SVM). As a result, the switching frequency is constant, and satisfactory control performance is achieved under both balanced and unbalanced network conditions. This technique achieves the control target of ensuring a constant stator-side active power, constant extended reactive power, and sinusoidal stator currents without power compensation terms or other measures under unbalanced network conditions. Different from other DPC-SVM methods, the phase-locked loop block is eliminated and the whole structure of the control system is simple and easy to use. No parameter needs to be tuned in the proposed method. The effectiveness of the proposed method is validated by the presented simulation and experimental results on a 1.5-kW laboratory DFIG control system.**

***Index Terms*—Generators, power control, predictive control, wind energy.**

I. Introduction

TO ADDRESS the increasing requirements on electric power, renewable energy power generation technologies have been widely considered. Among the novel variable energy power generation techniques, variable-speed constant-frequency wind energy conversion systems have rapidly gained popularity in the last few decades. Doubly fed induction generators (DFIGs) are the most widely used system in wind energy generators because a DFIG requires a power converter rated at only 25%–30% of the generator rating, therein being cost effective [1], [2].

Manuscript received November 11, 2018; revised January 26, 2019; accepted March 14, 2019. Date of publication March 17, 2019; date of current version September 6, 2019. This work was supported in part by the National Natural Science Foundation of China under Grant 51577003. A portion of this paper was presented at the 3rd International Future Energy Electronics Conference and ECCE Asia, Kaohsiung, Taiwan, 2017. Recommended for publication by Associate Editor Prof. L. Peng. *(Corresponding author: Yongchang Zhang.)*

Y. Zhang is with the Inverter Technologies Engineering Research Center of Beijing, North China University of Technology, Beijing 100144, China, and also with the Collaborative Innovation Center of Key Power Energy-Saving Technologies, Beijing 100871, China (e-mail:

under unbalanced network conditions. In [17], a low-complexity MPDPC for DFIGs is proposed. The calculation burdens are much reduced comparing with conventional MPDPC [7], [15]. Four control targets are achieved under unbalanced network conditions. However, the steady-state performance of the proposed method is worse than the multiple-vector-based MPDPC method proposed in [9] and [18].

Several DPC-SVM methods are proposed in [19]–[22] to achieve better control performance under unbalanced network conditions. In [19], a sliding-mode DPC (SM-DPC) strategy is proposed for DFIG under both balanced and unbalanced grid conditions using extended active power. SVM technique is combined with the SM-DPC method. The power ripples are eliminated in the proposed method under unbalanced network conditions. There are some parameters should be tuned, including integral parameters and the parameters of the switching control laws. The parameter-tuning processes make the methods in [19] difficult to use. In [20], a resonant-based back-stepping DPC strategy with SVM is proposed. Three control targets under unbalanced network conditions are achieved. However, back-stepping parameters and resonant parameters need to be tuned. Phase-locked loop is utilized to obtain the phase angle. Some variables have to be transformed to synchronous reference frame to realize three control targets. The structure of the control system is relatively complex. In [21], a DPC method of DFIG is proposed to eliminate oscillations of stator-side powers under the stator voltage balanced and unbalanced sags. The required rotor reference voltage is directly calculated based on the model of DFIG. Although constant stator powers are achieved under balanced and unbalanced voltage sags conditions, the stator currents are highly distorted under unbalanced stator voltages conditions. In [22], an SM-DPC is proposed for DFIG control system. SVM technique is combined with the SM-DPC method. However, three control targets are realized under unbalanced grid voltages. In the designing of the control law in sliding-mode method, the positive control gains and the boundary layer should be well designed. It is kind of complex in the practical applications.

In this paper, a new DPC method based on extended power theory [23]–[25] is proposed. A novel rotor voltage is calculated using the proposed DPC-SVM method. Without any power compensation terms, the proposed DPC-SVM method can be directly used under balanced and unbalanced network conditions. Under balanced network conditions, it achieves a satisfactory control performance equal to that of the DPC-SVM method based on conventional instantaneous power theory. Under unbalanced network conditions, this method achieves the control target of ensuring a constant stator-side active power and extended reactive power, as well as sinusoidal stator current. In the proposed DPC-SVM method, a constant switching frequency and satisfactory control performance are realized under both balanced and unbalanced network conditions. A preliminary study of the proposed method was presented in [26] and it was enhanced in this paper with detailed theoretical analysis and extensive experimental results. It is analytically derived that, by using the extended power theory, the power compensation value is zero. This explains in theory why the proposed method can achieve good performance without any power compensation. The effectiveness of the proposed method is validated by both simulation and experimental results from a 1.5-kW laboratory DFIG control system.

II. Dynamic Model of DFIG

A. Basic Equations of DFIG

The mathematical model of a DFIG described in a stationary reference frame can be expressed as [2]

$$\boldsymbol{u}_s = R_s \boldsymbol{i}_s + \frac{\mathrm{d}\boldsymbol{\psi}_s}{\mathrm{d}t} \tag{1}$$

$$\boldsymbol{u}_r = R_r \boldsymbol{i}_r + \frac{\mathrm{d}\boldsymbol{\psi}_r}{\mathrm{d}t} - \mathrm{j}\omega_r \psi_r \tag{2}$$

$$\boldsymbol{\psi}_s = L_s \boldsymbol{i}_s + L_m \boldsymbol{i}_r \tag{3}$$

$$\boldsymbol{\psi}_r = L_m \boldsymbol{i}_s + L_r \boldsymbol{i}_r \tag{4}$$

where $\boldsymbol{u}_s$, $\boldsymbol{u}_r$, $\boldsymbol{i}_s$, $\boldsymbol{i}_r$, $\boldsymbol{\psi}_s$, and $\boldsymbol{\psi}_r$ are the stator voltage vector, rotor voltage vector, stator current vector, rotor current vector, stator flux vector, and rotor flux vector, respectively; R_s, R_r, L_s, L_r, and L_m are the stator resistance, rotor resistance, stator inductance, rotor inductance, and mutual inductance, respectively; and ω_r is the electrical rotor speed.

From (3) and (4), the stator and rotor currents can be expressed using the stator and rotor fluxes as

$$\boldsymbol{i}_s = \lambda \left(L_r \boldsymbol{\psi}_s - L_m \boldsymbol{\psi}_r \right) \tag{5}$$

$$\boldsymbol{i}_r = \lambda \left(-L_m \boldsymbol{\psi}_s + L_s \boldsymbol{\psi}_r \right) \tag{6}$$

where $\lambda = 1/\left(L_s L_r - L_m^2 \right)$.

From (4) and (6), the rotor flux can be expressed by the stator flux and stator current, that is

$$\boldsymbol{\psi}_r = \frac{L_r}{L_m} \boldsymbol{\psi}_s - \frac{1}{\lambda L_m} \boldsymbol{i}_s. \tag{7}$$

According to the original power theory introduced in [27], the complex power vector $\boldsymbol{S}$ on the stator-side of the DFIG can be expressed as

$$\boldsymbol{S} = P_s + \mathrm{j} Q_s = \frac{3}{2} \boldsymbol{i}_s^* \cdot \boldsymbol{u}_s \tag{8}$$

where "$*$" is the conjugate operator of a complex vector.

The instantaneous active power P_s and reactive power Q_s can be expressed as the real and imaginary components of the complex power $\boldsymbol{S}$

$$P_s = \mathrm{Re}\left(\boldsymbol{S} \right) = \frac{3}{2} \mathrm{Re}\left(\boldsymbol{i}_s^* \boldsymbol{u}_s \right) \tag{9}$$

$$Q_s = \mathrm{Im}\left(\boldsymbol{S} \right) = \frac{3}{2} \mathrm{Im}\left(\boldsymbol{i}_s^* \boldsymbol{u}_s \right) \tag{10}$$

where the superscript "$*$" denotes the conjugate operator of a complex vector.

Extended reactive power theory is proposed in [23] and [24], where the extended reactive power is expressed as

$$Q_s^{\mathrm{nov}} = \frac{3}{2} \mathrm{Re}\left(\boldsymbol{i}_s^* \boldsymbol{u}_s' \right) \tag{11}$$

where the variable $\boldsymbol{u}'_s$ lags $\boldsymbol{u}_s$ by 90 electrical degrees, which is corresponding to a quarter of the fundamental period [28].

Under balanced network conditions, the extended reactive power can be expressed as

$$\begin{aligned} Q_s^{\text{nov}} &= \frac{3}{2}\text{Re}\left(\boldsymbol{i}_s^* \boldsymbol{u}'_s\right) = \frac{3}{2}\text{Re}\left(\boldsymbol{i}_s^* \cdot (-\text{j}\boldsymbol{u}_s)\right) \\ &= \frac{3}{2}\text{Im}\left(\boldsymbol{i}_s^* \boldsymbol{u}_s\right). \end{aligned} \tag{12}$$

Clearly, the extended reactive power is the same as the conventional reactive power under balanced network conditions.

B. Equations of DFIG Under Unbalanced Network Conditions

Under unbalanced network conditions, the stator voltage and stator current can be expressed as the sum of their respective positive sequence components (PSCs) and NSCs, i.e., [13]

$$\boldsymbol{u}_s = \boldsymbol{u}_s^+ + \boldsymbol{u}_s^- = \boldsymbol{u}_{sdq}^+ e^{\text{j}\omega_g t} + \boldsymbol{u}_{sdq}^- e^{-\text{j}\omega_g t} \tag{13}$$

$$\boldsymbol{i}_s = \boldsymbol{i}_s^+ + \boldsymbol{i}_s^- = \boldsymbol{i}_{sdq}^+ e^{\text{j}\omega_g t} + \boldsymbol{i}_{sdq}^- e^{-\text{j}\omega_g t} \tag{14}$$

where $\boldsymbol{u}_{sdq}^+ = u_{sd}^+ + \text{j}u_{sq}^+$, $\boldsymbol{u}_{sdq}^- = u_{sd}^- + \text{j}u_{sq}^-$, $\boldsymbol{i}_{sdq}^+ = i_{sd}^+ + \text{j}i_{sq}^+$, $\boldsymbol{i}_{sdq}^- = i_{sd}^- + \text{j}i_{sq}^-$, and ω_g is the fundamental grid frequency. The subscript "dq" represent the synchronous reference frame.

The delayed value of the unbalanced stator voltage $\boldsymbol{u}'_s$ and stator current $\boldsymbol{i}'_s$ can be expressed as

$$\begin{aligned} \boldsymbol{u}'_s &= \boldsymbol{u}_{sdq}^+ e^{\text{j}\left(\omega_g t - \frac{\pi}{2}\right)} + \boldsymbol{u}_{sdq}^- e^{-\text{j}\left(\omega_g t - \frac{\pi}{2}\right)} \\ &= -\text{j}\boldsymbol{u}_{sdq}^+ e^{\text{j}\omega_g t} + \text{j}\boldsymbol{u}_{sdq}^- e^{-\text{j}\omega_g t} \\ &= -\text{j}\boldsymbol{u}_s^+ + \text{j}\boldsymbol{u}_s^- \end{aligned} \tag{15}$$

$$\begin{aligned} \boldsymbol{i}'_s &= \boldsymbol{i}_{sdq}^+ e^{\text{j}\left(\omega_g t - \frac{\pi}{2}\right)} + \boldsymbol{i}_{sdq}^- e^{-\text{j}\left(\omega_g t - \frac{\pi}{2}\right)} \\ &= -\text{j}\boldsymbol{i}_{sdq}^+ e^{\text{j}\omega_g t} + \text{j}\boldsymbol{i}_{sdq}^- e^{-\text{j}\omega_g t} \\ &= -\text{j}\boldsymbol{i}_s^+ + \text{j}\boldsymbol{i}_s^-. \end{aligned} \tag{16}$$

Under unbalanced network conditions, the expressions of the stator active power and extended reactive power can be extended based on (9), (11), (13), (14), and (15), that is [26]

$$\begin{aligned} P_s &= \frac{3}{2}\text{Re}\left(\boldsymbol{i}_s^* \cdot \boldsymbol{u}_s\right) \\ &= \frac{3}{2}\text{Re}\left[\left(\boldsymbol{i}_{sdq}^+ \text{e}^{\text{j}\omega_g t} + \boldsymbol{i}_{sdq}^- \text{e}^{-\text{j}\omega_g t}\right)^* \right. \\ &\quad \left. \cdot \left(\boldsymbol{u}_{sdq}^+ \text{e}^{\text{j}\omega_g t} + \boldsymbol{u}_{sdq}^- \text{e}^{-\text{j}\omega_g t}\right)\right] \\ &= P_{s,0} + P_{s,\cos 2}\cos\left(2\omega_g t\right) + P_{s,\sin 2}\sin\left(2\omega_g t\right) \end{aligned} \tag{17}$$

$$\begin{aligned} Q_s^{\text{nov}} &= \frac{3}{2}\text{Re}\left(\boldsymbol{i}_s^* \cdot \boldsymbol{u}'_s\right) \\ &= \frac{3}{2}\text{Re}\left[\left(\boldsymbol{i}_{sdq}^+ \text{e}^{\text{j}\omega_g t} + \boldsymbol{i}_{sdq}^- \text{e}^{-\text{j}\omega_g t}\right)^* \right. \\ &\quad \left. \cdot \left(-\text{j}\boldsymbol{u}_{sdq}^+ \text{e}^{\text{j}\omega_g t} + \text{j}\boldsymbol{u}_{sdq}^- \text{e}^{-\text{j}\omega_g t}\right)\right] \\ &= Q_{s,0}^{\text{nov}} + Q_{s,\cos 2}^{\text{nov}}\cos\left(2\omega_g t\right) + Q_{s,\sin 2}^{\text{nov}}\sin\left(2\omega_g t\right) \end{aligned} \tag{18}$$

where

$$\begin{cases} P_{s,0} &= \frac{3}{2}\left(\boldsymbol{i}_{sdq}^+ \odot \boldsymbol{u}_{sdq}^+ + \boldsymbol{i}_{sdq}^- \odot \boldsymbol{u}_{sdq}^-\right) \\ P_{s,\cos 2} &= \frac{3}{2}\left(\boldsymbol{i}_{sdq}^+ \odot \boldsymbol{u}_{sdq}^- + \boldsymbol{i}_{sdq}^- \odot \boldsymbol{u}_{sdq}^+\right) \\ P_{s,\sin 2} &= \frac{3}{2}\left(\boldsymbol{i}_{sdq}^+ \otimes \boldsymbol{u}_{sdq}^- - \boldsymbol{i}_{sdq}^- \otimes \boldsymbol{u}_{sdq}^+\right) \\ Q_{s,0}^{\text{nov}} &= \frac{3}{2}\left(\boldsymbol{i}_{sdq}^+ \otimes \boldsymbol{u}_{sdq}^+ - \boldsymbol{i}_{sdq}^- \otimes \boldsymbol{u}_{sdq}^-\right) \\ Q_{s,\cos 2}^{\text{nov}} &= \frac{3}{2}\left(-\boldsymbol{i}_{sdq}^+ \otimes \boldsymbol{u}_{sdq}^- + \boldsymbol{i}_{sdq}^- \otimes \boldsymbol{u}_{sdq}^+\right) \\ Q_{s,\sin 2}^{\text{nov}} &= \frac{3}{2}\left(\boldsymbol{i}_{sdq}^+ \odot \boldsymbol{u}_{sdq}^- + \boldsymbol{i}_{sdq}^- \odot \boldsymbol{u}_{sdq}^+\right). \end{cases} \tag{19}$$

From (13), (14), (15), and (16), the PSCs and NSCs of stator voltage and stator current in the synchronous reference frame can be expressed by their original and delayed variables in the stationary reference frame, that is

$$\begin{bmatrix} \boldsymbol{u}_{sdq}^+ \\ \boldsymbol{u}_{sdq}^- \end{bmatrix} = \frac{1}{2}\begin{bmatrix} e^{-\text{j}\omega_g t} & \text{j}e^{-\text{j}\omega_g t} \\ e^{\text{j}\omega_g t} & -\text{j}e^{\text{j}\omega_g t} \end{bmatrix}\begin{bmatrix} \boldsymbol{u}_s \\ \boldsymbol{u}'_s \end{bmatrix} \tag{20}$$

$$\begin{bmatrix} \boldsymbol{i}_{sdq}^+ \\ \boldsymbol{i}_{sdq}^- \end{bmatrix} = \frac{1}{2}\begin{bmatrix} e^{-\text{j}\omega_g t} & \text{j}e^{-\text{j}\omega_g t} \\ e^{\text{j}\omega_g t} & -\text{j}e^{\text{j}\omega_g t} \end{bmatrix}\begin{bmatrix} \boldsymbol{i}_s \\ \boldsymbol{i}'_s \end{bmatrix}. \tag{21}$$

Substituting (20) and (21) into (19), (19) can be expressed using the original and delayed voltage and current signals under stationary reference frame

$$\begin{cases} P_{s,0} &= \frac{3}{4}\left(\boldsymbol{i}_s \odot \boldsymbol{u}_s + \boldsymbol{i}'_s \odot \boldsymbol{u}'_s\right) \\ P_{s,\cos 2} &= \frac{3}{4}\left(P_{s1}\cos\left(2\omega_g t\right) + P_{s2}\sin\left(2\omega_g t\right)\right) \\ P_{s,\sin 2} &= \frac{3}{4}\left(-P_{s2}\cos\left(2\omega_g t\right) + P_{s1}\sin\left(2\omega_g t\right)\right) \\ Q_{s,0}^{\text{nov}} &= \frac{3}{4}\left(\boldsymbol{i}_s \odot \boldsymbol{u}'_s - \boldsymbol{i}'_s \odot \boldsymbol{u}_s\right) \\ Q_{s,\cos 2}^{\text{nov}} &= \frac{3}{4}\left(P_{s2}\cos\left(2\omega_g t\right) - P_{s1}\sin\left(2\omega_g t\right)\right) \\ Q_{s,\sin 2}^{\text{nov}} &= \frac{3}{4}\left(P_{s1}\cos\left(2\omega_g t\right) + P_{s2}\sin\left(2\omega_g t\right)\right) \end{cases} \tag{22}$$

where

$$\begin{cases} P_{s1} &= \boldsymbol{i}_s \odot \boldsymbol{u}_s - \boldsymbol{i}'_s \odot \boldsymbol{u}'_s \\ P_{s2} &= \boldsymbol{i}_s \odot \boldsymbol{u}'_s + \boldsymbol{i}'_s \odot \boldsymbol{u}_s. \end{cases} \tag{23}$$

III. Principle of Conventional DPC-SVM and Proposed DPC-SVM

A. Overall Control Diagram of Two Methods

Fig. 1(a) illustrates the overall control diagram of the conventional DPC-SVM method [9], [12], including the 3/2 transformation of the stator voltages/currents, power calculation block, rotor voltage vector calculation, and SVM block. The overall control diagram of the proposed DPC-SVM is presented in Fig. 1(b). The second-order generalized integrator (SOGI) [29] is utilized to obtain the original stator voltages and delayed stator voltages. The stator-side active power and extended reactive power are calculated in the stator-side power calculation block. On the basis of the delayed stator voltages, extended stator-side reactive power, and other variables of the DFIG, the rotor reference voltage is calculated by the proposed DPC-SVM method. The details of the conventional DPC-SVM and the proposed DPC-SVM are explained in the following.

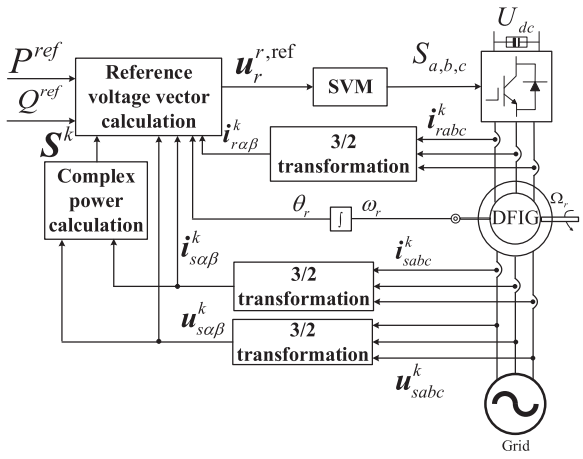

(a)

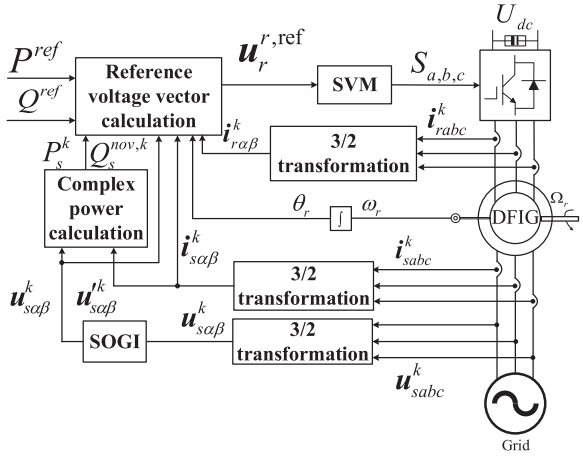

(b)

Fig. 1. Control diagram of (a) conventional DPC-SVM and (b) the proposed DPC-SVM.

B. Conventional DPC-SVM

Under ideal network conditions, the derivative of the complex power can be obtained from (1), (2), (3), and (4) as [2], [9]

$$\begin{aligned}\frac{\mathrm{d}\boldsymbol{S}}{dt} &= 1.5\left(\boldsymbol{i}_s^*\frac{\mathrm{d}\boldsymbol{u}_s}{\mathrm{d}t}+\frac{\mathrm{d}\boldsymbol{i}_s^*}{\mathrm{d}t}\boldsymbol{u}_s\right)\\ &= -\left(\lambda L_r R_s-\mathrm{j}\omega_{sl}\right)\boldsymbol{S}+1.5\left(\lambda L_r\left|\boldsymbol{u}_s\right|^2\right.\\ &\quad\left.-\lambda L_m\left(\boldsymbol{u}_r^*-R_r\boldsymbol{i}_r^*\right)\boldsymbol{u}_s+\mathrm{j}\lambda L_r\omega_r\left(\boldsymbol{\psi}_s^*\boldsymbol{u}_s\right)\right)\end{aligned}\tag{24}$$

where $\lambda=1/\left(L_sL_r-L_m^2\right)$ and $\omega_{sl}=\omega_g-\omega_r$ is the slip speed.

The derivative of the stator-side complex power in (24) can be discretized using the first-order Euler method, that is

$$\left(\frac{\mathrm{d}\boldsymbol{S}}{\mathrm{d}t}\right)^k=\frac{\boldsymbol{S}^{k+1}-\boldsymbol{S}^k}{T_{sc}}\tag{25}$$

where T_{sc} is the sampling period of the control system, the superscripts "k" and "$k+1$" represent the kth and $k+1$th sampling instant.

The aim of the conventional DPC-SVM is to achieve deadbeat control of the complex power, namely, $\boldsymbol{S}^{\mathrm{ref}}=\boldsymbol{S}^{k+1}$. Substituting (25) into (24), (24) can be expressed as

$$\begin{aligned}\frac{\boldsymbol{S}^{\mathrm{ref}}-\boldsymbol{S}^k}{T_{sc}} &= -\left(\lambda L_rR_s-\mathrm{j}\omega_{sl}^k\right)\boldsymbol{S}^k+1.5\left(\lambda L_r\left|\boldsymbol{u}_s^k\right|^2\right.\\ &\quad-\lambda L_m\left(\left(\boldsymbol{u}_r^{\mathrm{ref}}\right)^*-R_r\left(\boldsymbol{i}_r^k\right)^*\right)\boldsymbol{u}_s^k\\ &\quad\left.+\mathrm{j}\lambda L_r\omega_r^k\left(\left(\boldsymbol{\psi}_s^k\right)^*\boldsymbol{u}_s^k\right)\right)\end{aligned}\tag{26}$$

where T_{sc} is the control period.

Solving (26), the desired rotor converter voltage vector can be obtained as

$$\begin{aligned}\boldsymbol{u}_r^{\mathrm{ref}} &= \frac{2\left(S^k-S^{\mathrm{ref}}\right)^*}{3\lambda L_mT_{sc}\left(\boldsymbol{u}_s^k\right)^*}+\frac{L_r}{L_m}\boldsymbol{u}_s^k-\frac{\left(\lambda L_rR_s+\mathrm{j}\omega_{sl}^k\right)}{\lambda L_m}\boldsymbol{i}_s^k\\ &\quad-\frac{\mathrm{j}L_r\omega_r^k}{L_m}\boldsymbol{\psi}_s^k+R_r\boldsymbol{i}_r^k.\end{aligned}\tag{27}$$

Finally, the rotor reference voltage is supposed to be transformed from the stationary reference frame to the rotor reference frame, and the ultimate required rotor voltage $\boldsymbol{u}_r^{r,\mathrm{ref}}$ is obtained, that is

$$\boldsymbol{u}_r^{r,\mathrm{ref}}=\boldsymbol{u}_r^{\mathrm{ref}}\cdot e^{-\mathrm{j}\theta_r}$$

where θ_r is the rotor electrical angle and the superscript "r" denotes the rotor reference frame.

C. Proposed DPC-SVM

Under balanced network conditions, (12) shows that the extended reactive power is the same as the conventional reactive power. Therefore, there is no difference between the conventional DPC-SVM method and the proposed DPC-SVM method under balanced network conditions. Under unbalanced network conditions, from (13) and (15), the differentiation of the stator voltage vector and its delayed value in the stationary reference frame can be obtained as

$$\frac{\mathrm{d}\boldsymbol{u}_s}{\mathrm{d}t}=\mathrm{j}\omega_g\boldsymbol{u}_s^+-\mathrm{j}\omega_g\boldsymbol{u}_s^-=-\omega_g\boldsymbol{u}_s'\tag{28}$$

$$\frac{\mathrm{d}\boldsymbol{u}_s'}{\mathrm{d}t}=\omega_g\boldsymbol{u}_s^++\omega_g\boldsymbol{u}_s^-=\omega_g\boldsymbol{u}_s.\tag{29}$$

As is mentioned before, the original stator voltages and delayed stator voltages are directly obtained by the SOGI [29] under unbalanced network conditions. The main diagram of SOGI is illustrated in Fig. 2. The input of the SOGI is the stator voltage vector $\boldsymbol{u}_s$. The output of the SOGI is the filtered stator voltage $\boldsymbol{u}_{sf}$ and one-quarter fundamental period delayed variable $\boldsymbol{u}_{sf}'$.

The transfer function of SOGI can be expressed as

$$D\left(s\right)=\frac{\boldsymbol{u}_{sf}\left(s\right)}{\boldsymbol{u}_s\left(s\right)}=\frac{k\omega s}{s^2+k\omega s+\omega^2}\tag{30}$$

$$Q\left(s\right)=\frac{\boldsymbol{u}_{sf}'\left(s\right)}{\boldsymbol{u}_s\left(s\right)}=\frac{k\omega^2}{s^2+k\omega s+\omega^2}\tag{31}$$

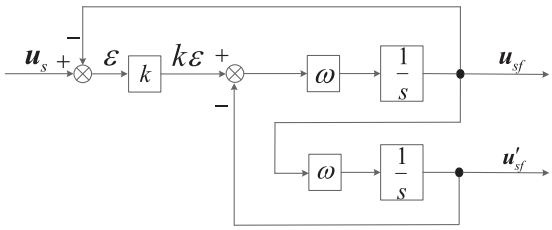

Fig. 2. Diagram of SOGI.

where k is the gain constant, which is set to $\sqrt{2}$ in this paper. ω is the fundamental frequency of the grid voltage, which is 50 Hz in this paper.

The differentiation of the stator current can be obtained from (5) as

$$\frac{\mathrm{d}\boldsymbol{i}_s}{\mathrm{d}t} = \lambda\left(L_r\frac{\mathrm{d}\boldsymbol{\psi}_s}{\mathrm{d}t} - L_m\frac{\mathrm{d}\boldsymbol{\psi}_r}{\mathrm{d}t}\right). \tag{32}$$

From (1), (2), (9), (11), (28), and (32), the differential of the active power can be obtained as

$$\begin{aligned}\frac{\mathrm{d}P_s}{\mathrm{d}t} &= 1.5\lambda L_r\left|\boldsymbol{u}_s\right|^2 - 1.5\lambda L_m\mathrm{Re}\left(\boldsymbol{u}_s\boldsymbol{u}_r^*\right)\\ &\quad + 1.5\lambda L_m R_r\mathrm{Re}\left(\boldsymbol{i}_r^*\boldsymbol{u}_s\right) - 1.5\lambda L_r\omega_r\mathrm{Im}\left(\boldsymbol{u}_s\psi_s^*\right)\\ &\quad + 1.5\omega_r\mathrm{Im}\left(\boldsymbol{i}_s^*\boldsymbol{u}_s\right) - \lambda R_sL_rP_s - \omega_gQ_s^{\mathrm{nov}}.\end{aligned} \tag{33}$$

Similarly, the differential of the extended reactive power can be obtained from (1), (2), (9), (11), (29), and (32). Specifically

$$\begin{aligned}\frac{\mathrm{d}Q_s^{\mathrm{nov}}}{\mathrm{d}t} &= 1.5\lambda L_r\mathrm{Re}\left(\boldsymbol{u}'_s\boldsymbol{u}_s^*\right) - 1.5\lambda L_m\mathrm{Re}\left(\boldsymbol{u}'_s\boldsymbol{u}_r^*\right)\\ &\quad + 1.5\lambda L_m R_r\mathrm{Re}\left(\boldsymbol{i}_r^*\boldsymbol{u}'_s\right) - 1.5\lambda L_r\omega_r\mathrm{Im}\left(\boldsymbol{u}'_s\boldsymbol{\psi}_s^*\right)\\ &\quad + 1.5\omega_r\mathrm{Im}\left(\boldsymbol{i}_s^*\boldsymbol{u}'_s\right) + \omega_gP_s - \lambda R_sL_rQ_s^{\mathrm{nov}}.\end{aligned} \tag{34}$$

On the basis of the first-order Euler method, the derivative of the stator-side complex power in (33) and (34) can be discretized as

$$\left(\frac{\mathrm{d}P_s}{\mathrm{d}t}\right)^k = \frac{P_s^{k+1}-P_s^k}{T_{sc}}$$

$$\left(\frac{\mathrm{d}Q_s^{\mathrm{nov}}}{\mathrm{d}t}\right)^k = \frac{Q_s^{nov,k+1}-Q_s^{nov,k}}{T_{sc}}.$$

Similar to (26), the stator-side active power and extended reactive power in the next instant are replaced by their reference values. Then, (33) and (34) can be expressed as

$$\begin{aligned}\frac{1}{T_{sc}}\begin{bmatrix}P_s^{\mathrm{ref}}-P_s^k\\ Q_s^{\mathrm{ref}}-Q_s^{nov,k}\end{bmatrix} &= \frac{3\lambda L_r}{2}\begin{bmatrix}u_{s\alpha}^ku_{s\alpha}^k+u_{s\beta}^ku_{s\beta}^k\\ u_{s\alpha}'^ku_{s\alpha}^k+u_{s\beta}'^ku_{s\beta}^k\end{bmatrix}\\ &\quad - \frac{3\lambda L_r\omega_r}{2}\begin{bmatrix}u_{s\beta}^k\psi_{s\alpha}^k-u_{s\alpha}^k\psi_{s\beta}^k\\ u_{s\beta}'^k\psi_{s\alpha}^k-u_{s\alpha}'^k\psi_{s\beta}^k\end{bmatrix}\\ &\quad + \frac{3\lambda L_mR_r}{2}\begin{bmatrix}i_{r\alpha}^ku_{s\alpha}^k+i_{r\beta}^ku_{s\beta}^k\\ i_{r\alpha}^ku_{s\alpha}'^k+i_{r\beta}^ku_{s\beta}'^k\end{bmatrix}\\ &\quad - \frac{3\lambda L_m}{2}\begin{bmatrix}u_{s\alpha}^k & u_{s\beta}^k\\ u_{s\alpha}'^k & u_{s\beta}'^k\end{bmatrix}\begin{bmatrix}u_{r\alpha}^k\\ u_{r\beta}^k\end{bmatrix}\\ &\quad + 1.5\omega_r\begin{bmatrix}u_{s\beta}^ki_{s\alpha}^k-u_{s\alpha}^ki_{s\beta}^k\\ u_{s\beta}'^ki_{s\alpha}^k-u_{s\alpha}'^ki_{s\beta}^k\end{bmatrix}\\ &\quad + \begin{bmatrix}-\lambda R_sL_r & -\omega_g^k\\ \omega_g^k & -\lambda R_sL_r\end{bmatrix}\begin{bmatrix}P_s^k\\ Q_s^{nov,k}\end{bmatrix}\end{aligned} \tag{35}$$

where the subscripts "α" and "β" represent the α-axis and β-axis of the stationary reference frame.

Solving (35), the final rotor-side reference voltage is calculated as

$$\begin{aligned}\begin{bmatrix}u_{r\alpha}^k\\ u_{r\beta}^k\end{bmatrix} &= -\frac{2}{3\lambda L_mT_{sc}\sigma}\begin{bmatrix}u_{s\beta}'^k & -u_{s\beta}^k\\ -u_{s\alpha}'^k & u_{s\alpha}^k\end{bmatrix}\begin{bmatrix}P_s^{\mathrm{ref}}-P_s^k\\ Q_s^{\mathrm{ref}}-Q_s^{nov,k}\end{bmatrix}\\ &\quad + \frac{L_r}{L_m\sigma}\begin{bmatrix}u_{s\beta}'^k & -u_{s\beta}^k\\ -u_{s\alpha}'^k & u_{s\alpha}^k\end{bmatrix}\begin{bmatrix}u_{s\alpha}^ku_{s\alpha}^k+u_{s\beta}^ku_{s\beta}^k\\ u_{s\alpha}'^ku_{s\alpha}^k+u_{s\beta}'^ku_{s\beta}^k\end{bmatrix}\\ &\quad - \frac{L_r\omega_r}{L_m\sigma}\begin{bmatrix}u_{s\beta}'^k & -u_{s\beta}^k\\ -u_{s\alpha}'^k & u_{s\alpha}^k\end{bmatrix}\begin{bmatrix}u_{s\beta}^k\psi_{s\alpha}^k-u_{s\alpha}^k\psi_{s\beta}^k\\ u_{s\beta}'^k\psi_{s\alpha}^k-u_{s\alpha}'^k\psi_{s\beta}^k\end{bmatrix}\\ &\quad + \frac{R_r}{\sigma}\begin{bmatrix}u_{s\beta}'^k & -u_{s\beta}^k\\ -u_{s\alpha}'^k & u_{s\alpha}^k\end{bmatrix}\begin{bmatrix}i_{r\alpha}^ku_{s\alpha}^k+i_{r\beta}^ku_{s\beta}^k\\ i_{r\alpha}^ku_{s\alpha}'^k+i_{r\beta}^ku_{s\beta}'^k\end{bmatrix}\\ &\quad + \frac{\omega_r}{\lambda L_m\sigma}\begin{bmatrix}u_{s\beta}'^k & -u_{s\beta}^k\\ -u_{s\alpha}'^k & u_{s\alpha}^k\end{bmatrix}\begin{bmatrix}u_{s\beta}^ki_{s\alpha}^k-u_{s\alpha}^ki_{s\beta}^k\\ u_{s\beta}'^ki_{s\alpha}^k-u_{s\alpha}'^ki_{s\beta}^k\end{bmatrix}\\ &\quad + \frac{2}{3\lambda L_m\sigma}\begin{bmatrix}u_{s\beta}'^k & -u_{s\beta}^k\\ -u_{s\alpha}'^k & u_{s\alpha}^k\end{bmatrix}\begin{bmatrix}-\lambda R_sL_r & -\omega_g^k\\ \omega_g^k & -\lambda R_sL_r\end{bmatrix}\\ &\quad \cdot\begin{bmatrix}P_s^k\\ Q_s^{nov,k}\end{bmatrix}\end{aligned} \tag{36}$$

where $\sigma = u_{s\alpha}^ku_{s\beta}'^k - u_{s\alpha}'^ku_{s\beta}^k$

$$\boldsymbol{u}_r^{\mathrm{ref}} = u_{r\alpha}^k + \mathrm{j}u_{r\beta}^k. \tag{37}$$

Similarly, the rotor reference voltage vector is supposed to be transformed from the stationary reference frame to the rotor reference frame. The final calculated rotor reference voltage vector $\boldsymbol{u}_r^{r,\mathrm{ref}}$ is as follows:

$$\boldsymbol{u}_r^{r,\mathrm{ref}} = \boldsymbol{u}_r^{\mathrm{ref}}\cdot e^{-\mathrm{j}\theta_r} \tag{38}$$

D. Power Analysis Under Unbalanced Network Conditions

Under unbalanced network conditions, due to the extended reactive power is used in the proposed DPC-SVM method, constant stator-side active power and extended reactive power can be realized under the assumption that stator currents are sinusoidal but unbalanced. That also means that the stator currents

only contain fundamental components without other harmonics under unbalanced network conditions in the proposed DPC-SVM. However, under unbalanced network conditions, the stator currents will be distorted when constant stator-side powers are achieved in the conventional DPC-SVM. The detailed explanations are presented in this section.

From (19), the control target of the proposed DPC-SVM under unbalanced network conditions can be expressed by the equation set, that is

$$\begin{cases} P_{s,0} & = P_s^{\text{ref}} \\ P_{s,\cos 2} & = 0 \\ P_{s,\sin 2} & = 0 \\ Q_{s,0}^{\text{nov}} & = Q_s^{\text{ref}} \\ Q_{s,\cos 2}^{\text{nov}} & = 0 \\ Q_{s,\sin 2}^{\text{nov}} & = 0. \end{cases} \tag{39}$$

It is observed in (19) that

$$\begin{cases} P_{s,\cos 2} = & Q_{s,\sin 2}^{\text{nov}} \\ P_{s,\sin 2} = & -Q_{s,\cos 2}^{\text{nov}}. \end{cases} \tag{40}$$

The two oscillation terms of extended reactive power in (39) can be removed. The six equations proposed for solving the required reference stator currents are reduced to four equations. Four stator current components need to be solved, that is: $i_{sd}^{+}, i_{sq}^{+}, i_{sd}^{-}, i_{sq}^{-}$. It denotes that the injecting NSCs of stator currents is sufficient and necessary to obtain constant values of stator-side active power and extended reactive power under unbalanced network conditions in the proposed DPC-SVM method. From (19), (20), (21), (39), and (40), the reference stator currents can be calculated as

$$\boldsymbol{i}_s^{\text{ref}} = \frac{-2\text{j}\boldsymbol{u}_s'}{3\left(\boldsymbol{u}_s \otimes \boldsymbol{u}_s'\right)} \cdot P_s^{\text{ref}} + \frac{2\text{j}\boldsymbol{u}_s}{3\left(\boldsymbol{u}_s \otimes \boldsymbol{u}_s'\right)} \cdot Q_s^{\text{ref}}. \tag{41}$$

No other current harmonics need to be injected to keep the constant stator-side powers. Therefore, the distortion on the stator-side currents will be eliminated under unbalanced network conditions. The stator-side currents are sinusoidal but unbalanced because the NSCs are contained in the currents.

While in the conventional DPC-SVM, from (10), (13), and (14), the constant value and oscillation terms of conventional stator-side reactive power can be expressed as

$$\begin{cases} Q_{s,0} & = \frac{3}{2}\left(\boldsymbol{i}_{sdq}^{+} \otimes \boldsymbol{u}_{sdq}^{+} + \boldsymbol{i}_{sdq}^{-} \otimes \boldsymbol{u}_{sdq}^{-}\right) \\ Q_{s,\cos 2} & = \frac{3}{2}\left(\boldsymbol{i}_{sdq}^{+} \otimes \boldsymbol{u}_{sdq}^{-} + \boldsymbol{i}_{sdq}^{-} \otimes \boldsymbol{u}_{sdq}^{+}\right) \\ Q_{s,\sin 2} & = \frac{3}{2}\left(-\boldsymbol{i}_{sdq}^{+} \odot \boldsymbol{u}_{sdq}^{-} + \boldsymbol{i}_{sdq}^{-} \odot \boldsymbol{u}_{sdq}^{+}\right). \end{cases} \tag{42}$$

TABLE I
CONTROL AND MACHINE PARAMETERS

DC bus voltage (V)	U_{dc}	100
Sampling frequency (kHz)	f_{sc}	10
Stator/rotor turn ratio	N	3.36
Rated power (kW)	P_N	1.5
Grid voltage (V)	U_N	212
Rated frequency (Hz)	f_N	50
Number of motor pairs	N_p	3
Stator resistance (Ω)	R_s	4.570
Rotor resistance (Ω)	R_r	3.228
Mutual inductance (mH)	L_m	214.57
Stator inductance (mH)	L_s	225.40
Rotor inductance (mH)	L_r	225.40

Keeping constant stator-side powers in conventional DPC-SVM means that

$$\begin{cases} P_{s,0} & = P_s^{\text{ref}} \\ P_{s,\cos 2} & = 0 \\ P_{s,\sin 2} & = 0 \\ Q_{s,0} & = Q_s^{\text{ref}} \\ Q_{s,\cos 2} & = 0 \\ Q_{s,\sin 2} & = 0. \end{cases} \tag{43}$$

The power oscillation terms do not satisfy the relationship that is proposed in (40). Therefore, all six equations are required to solve the four current components in conventional DPC-SVM method. The feasible solution to the four variables $(i_{sd}^{+}, i_{sq}^{+}, i_{sd}^{-}, i_{sq}^{-})$ cannot be obtained. Other than the PSCs and NSCs, current harmonics will be injected in the stator currents to obtain constant stator-side powers under unbalanced network conditions. So when the control target of keeping constant active power and reactive power are realized, the stator currents in conventional DPC-SVM are distorted under unbalanced network conditions.

IV. SIMULATION AND EXPERIMENTAL RESULTS

A. Simulation Results

In this section, all the simulation results of the conventional DPC-SVM method and of the proposed DPC-SVM method are presented. The conventional DPC-SVM and proposed DPC-SVM methods are simulated in MATLAB/Simulink for a 1.5-kW DFIG control system. The machine parameters of the DFIG are shown in Table I. In addition, the simulation results from conventional DPC-SVM are presented for comparison. The sampling frequencies of the conventional DPC-SVM and proposed DPC-SVM method are 10 kHz.

Fig. 3 shows the simulation results of two DPC methods when the network condition changes from balanced to unbalanced. From top to bottom, the curves shown in Fig. 3 are the stator-side active power, stator-side conventional reactive power, stator-side extended reactive power, stator currents, rotor currents, three-phase grid voltages, and electromagnetic torque.

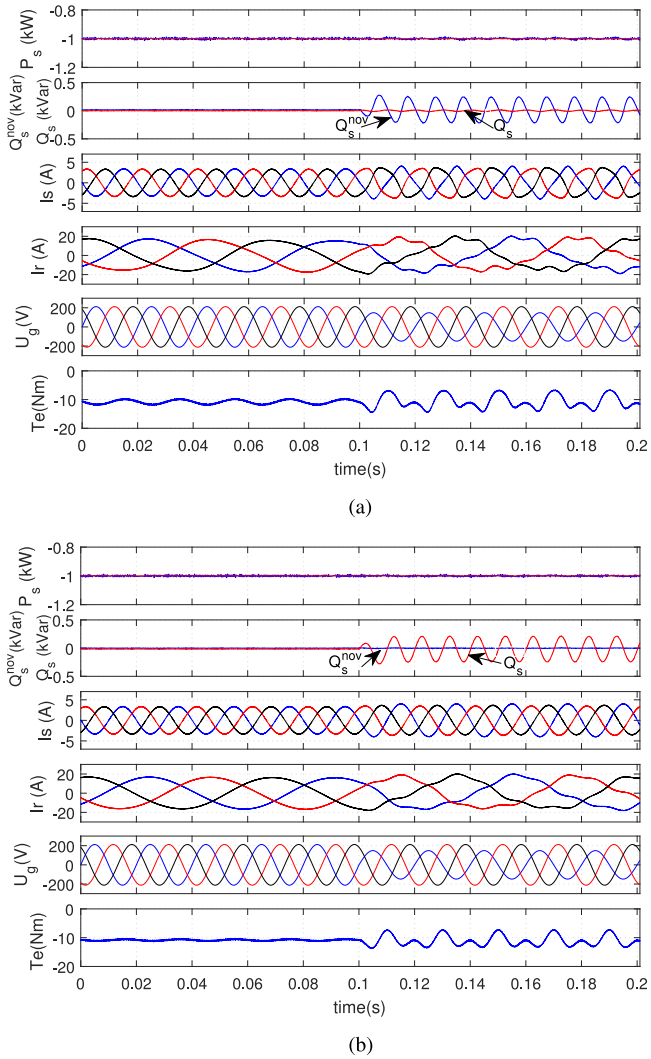

Fig. 3. Simulation results of two DPC methods when the network condition changes from balanced to unbalanced. (a) Conventional DPC-SVM. (b) Proposed DPC-SVM.

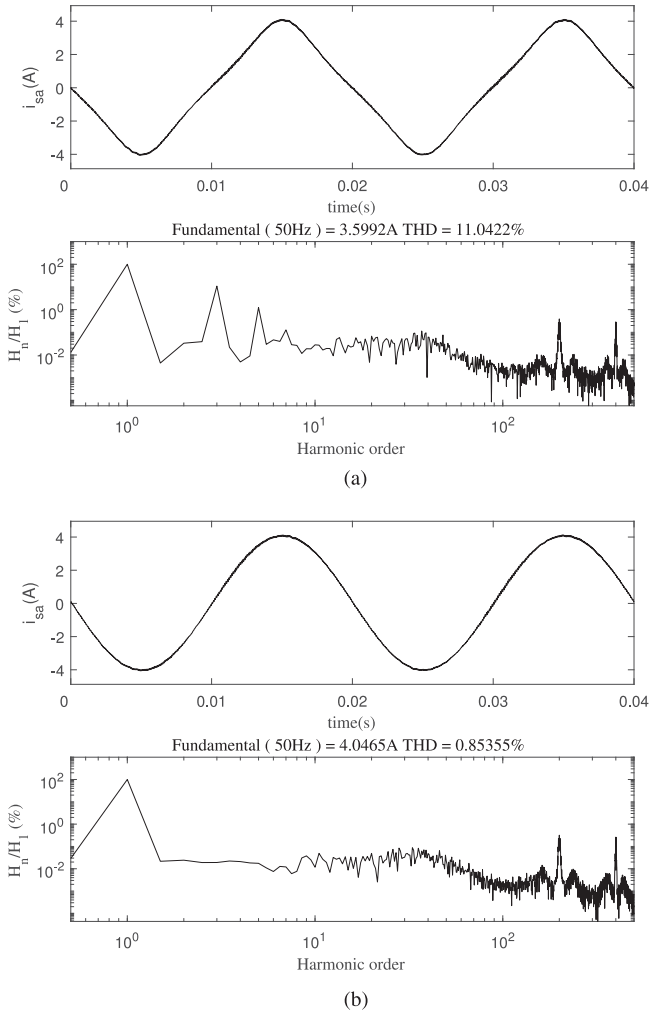

Fig. 4. Simulated harmonic spectra analysis of stator currents under the unbalanced network condition. (a) Conventional DPC-SVM. (b) Proposed DPC-SVM.

Two types of reactive powers are plotted in one channel for comparison. Fig. 3(a) shows the control performance of conventional DPC-SVM when the grid voltage changes from balanced to unbalanced. At 0.1 s, the phase A grid voltage decreases from 212 V to 70%, 148.4 V. It can be observed in Fig. 3(a) that when the network condition becomes unbalanced, the real stator-side power closely tracks its reference value. In addition, in the stator-side reactive power channel, the extended reactive power oscillates when the grid voltage is unbalanced. Moreover, the stator currents and rotor currents are severely distorted under the unbalanced network conditions. Fig. 3(b) shows the control performance of the proposed DPC-SVM method when the network voltage changes from balanced to unbalanced. In Fig. 3(b), the stator-side active power and extended reactive power track their reference values closely. The conventional stator-side reactive power oscillates when the network condition is unbalanced. Under the unbalanced network condition, three-phase stator currents are sinusoidal. It can be found in Fig. 3 that there is some impact on the torque oscillation range of DFIG in the proposed DPC-SVM method when compared with conventional DPC-SVM. The oscillation range is relatively small in the proposed DPC-SVM method than that of conventional DPC-SVM method. The harmonic spectra analysis of the stator currents under the two DPC methods is presented in Fig. 4. In the conventional DPC-SVM method, the total harmonic distortion (THD) of the phase A stator current is 11.04% under unbalanced network conditions. However, the THD of the phase A stator current under the proposed DPC-SVM method is 0.85% when the network is unbalanced.

Fig. 5 shows the simulation results of two DPC-SVM methods when the network conditions change from unbalanced to unbalanced and distorted network conditions. Fig. 5(a) shows the simulation results of conventional DPC-SVM method when the network conditions change from unbalanced to unbalanced and distorted. In Fig. 5(a), phase A grid voltage dips from 212 V to its 50%, 106 V at first. Then, 10% fifth-order harmonic component and 10% seventh-order harmonic component are added to the grid voltage at 0.1 s. It is observed that when the network

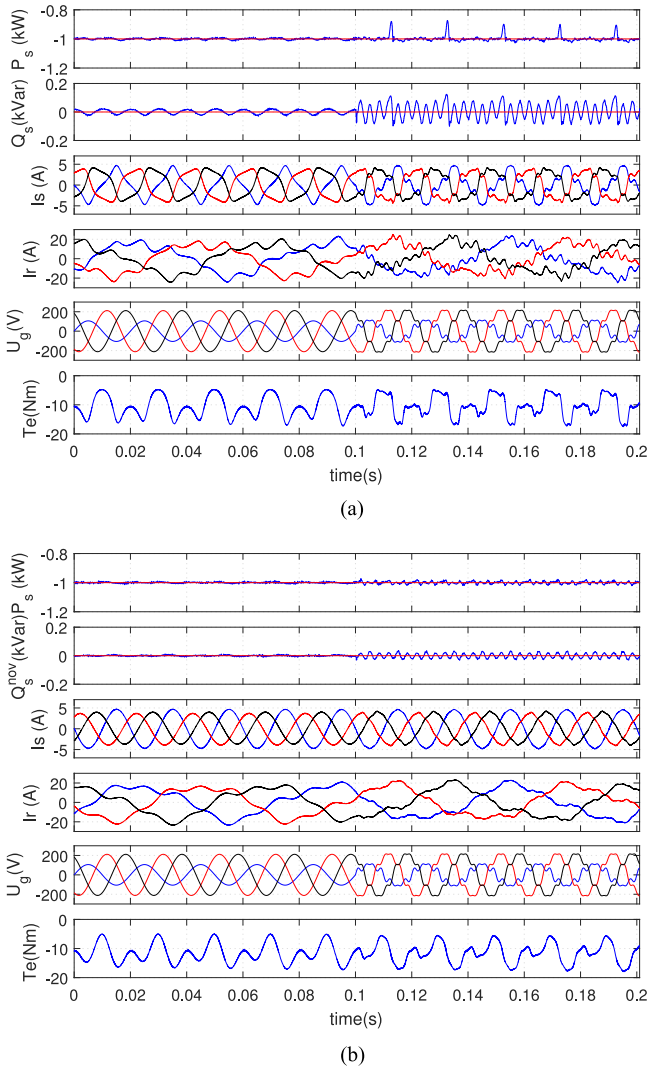

Fig. 5. Simulated steady-state responses of two DPC methods when the network conditions change from unbalanced to unbalanced and distorted. (a) Conventional DPC-SVM. (b) Proposed DPC-SVM.

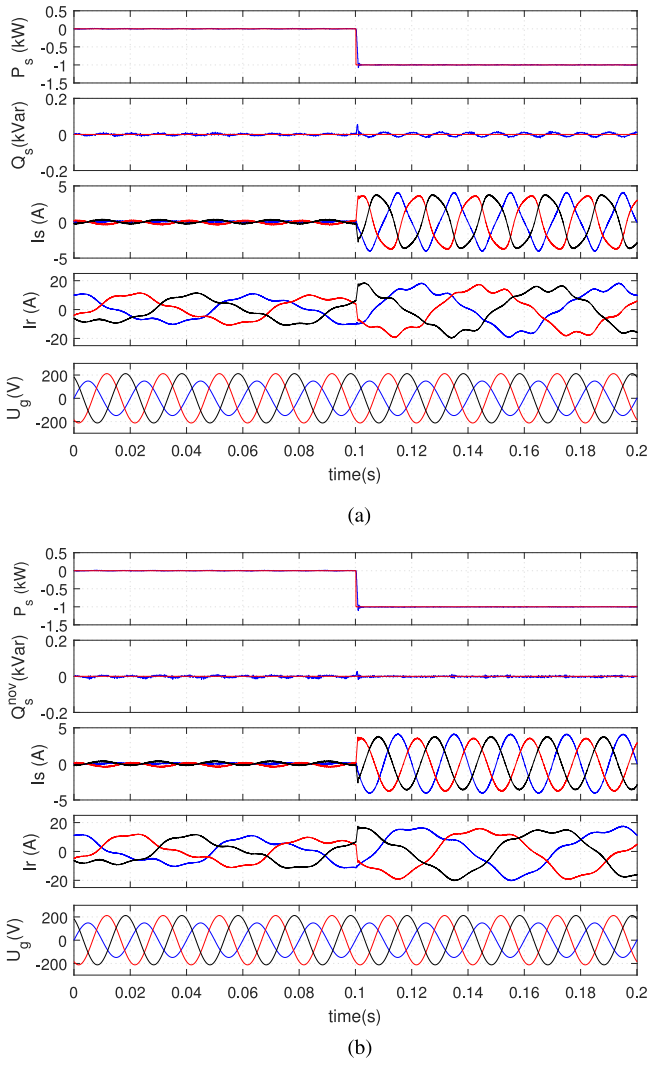

Fig. 6. Simulated dynamic responses of two methods when P_s^{ref} increases from 0 to -1000 W. (a) Conventional DPC-SVM. (b) Proposed DPC-SVM.

conditions change from unbalanced to unbalanced and distorted, substantial harmonic components emerged in the stator currents, rotor currents, and stator-side powers. Fig. 5(b) shows the simulation results of the proposed DPC-SVM method. Compared to conventional DPC-SVM, the harmonic components are much reduced in the stator currents, rotor currents, stator-side powers, and electromagnetic torque. However, there are still some distortion in the stator currents and rotor currents. More work needs to be done to extend the proposed method to the condition of unbalanced and distorted network. As this part of work is out of scope of this paper, it is not further expanded here and may be studied in the future.

Fig. 6 shows the dynamic responses of two methods when the reference value of the stator-side active power P_s^{ref} changes stepwise from 0 to -1000 W. In Fig. 6(a), when the reference value of the stator-side active power changes under the conventional DPC-SVM method, the real value of the active power perfectly tracks its reference value. In addition, the real value of the stator-side active power follows its reference value closely when the reference value of the active power changes. However, after the active power changes, the stator currents are severely distorted. In Fig. 6(b), when the reference value of the stator-side active power changes from 0 to -1000 W, the real active power also perfectly follows. In addition, the real value of the extended reactive power closely tracks its reference value without any oscillations. The stator currents are sinusoidal after 0.1 s, which is different from the distorted stator currents in the conventional DPC-SVM method.

Fig. 7 compares the dynamic responses of the two DPC-SVM methods when the rotor speed changes from 700 (slip s $= 0.3$) to 1300 r/min (slip s $= -0.3$). The speed range almost coincides with the possible operating range of the DFIG. In the conventional DPC-SVM method, the real values of the stator-side power track their reference value closely in Fig. 7(a), but the stator currents are distorted. It is highly inappropriate to directly

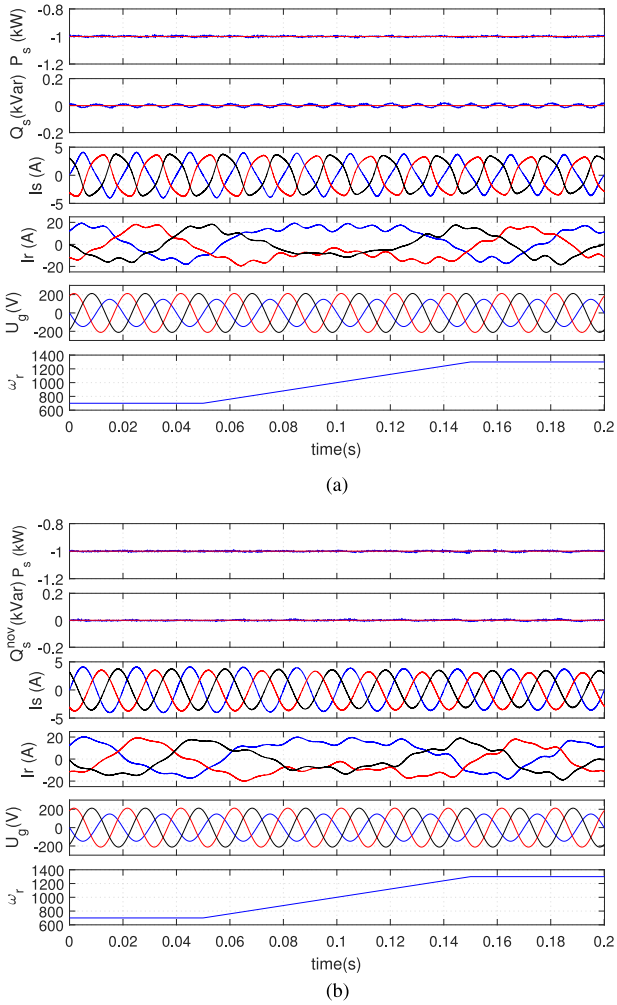

Fig. 7. Simulated dynamic responses of two DPC methods when the rotor speed changes from 700 to 1300 r/min. (a) Conventional DPC-SVM. (b) Proposed DPC-SVM.

use the conventional DPC-SVM method in the control system of a DFIG under unbalanced network conditions because the quality of the stator current is one of the most important requirements of the grid operator. However, in Fig. 7(b), the real values of the stator-side active power and extended reactive power closely track their reference values. The three-phase stator currents are sinusoidal under unbalanced network conditions, even when the rotor speed changes in a large range.

Fig. 8 shows the control performance of proposed DPC-SVM method under unbalanced network conditions when the estimated stator resistance R_s, rotor resistance R_r, and mutual inductance L_m vary from 70% to 130% of their nominal values. The parameter k is the ratio of estimated parameter in the controller to its nominal value, it increases 10% after every 0.05 s in Fig. 8. In Fig. 8(a), the deviation of stator resistance has a little influence on the real value of stator-side active power. The steady-state error of the active power is within ± 20 W when the stator resistance varies from 70% to 130% of its nominal value. Such error is negligible when comparing with

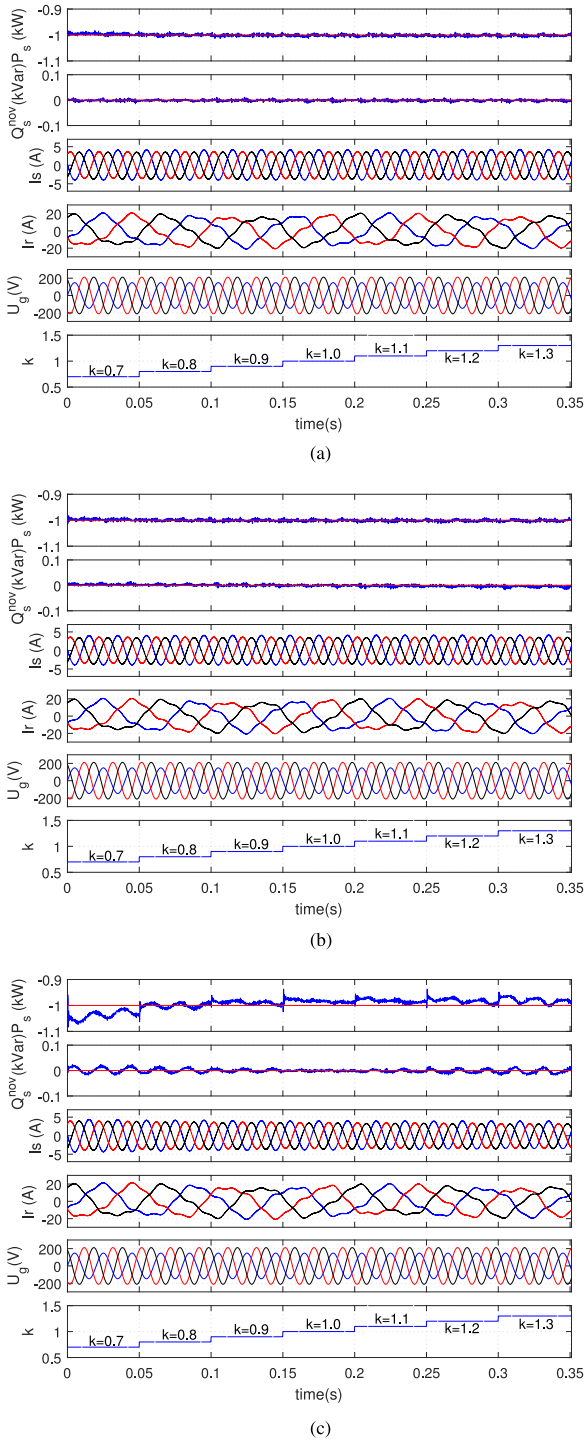

Fig. 8. Simulation results of proposed DPC-SVM method under unbalanced network conditions when the machine parameters vary from 70% to 130% of their nominal values. (a) Stator resistance R_s varies. (b) Rotor resistance R_r varies. (c) Mutual inductance L_m varies.

the reference value, -1000 W. In Fig. 8(b), the steady-state errors of stator-side active power and reactive power are produced when the rotor resistance varies. The values of the stator-side power errors between the real values and the reference values are small. In Fig. 8(b), when the mutual inductance changes, the steady-state errors of stator-side active power are produced. The

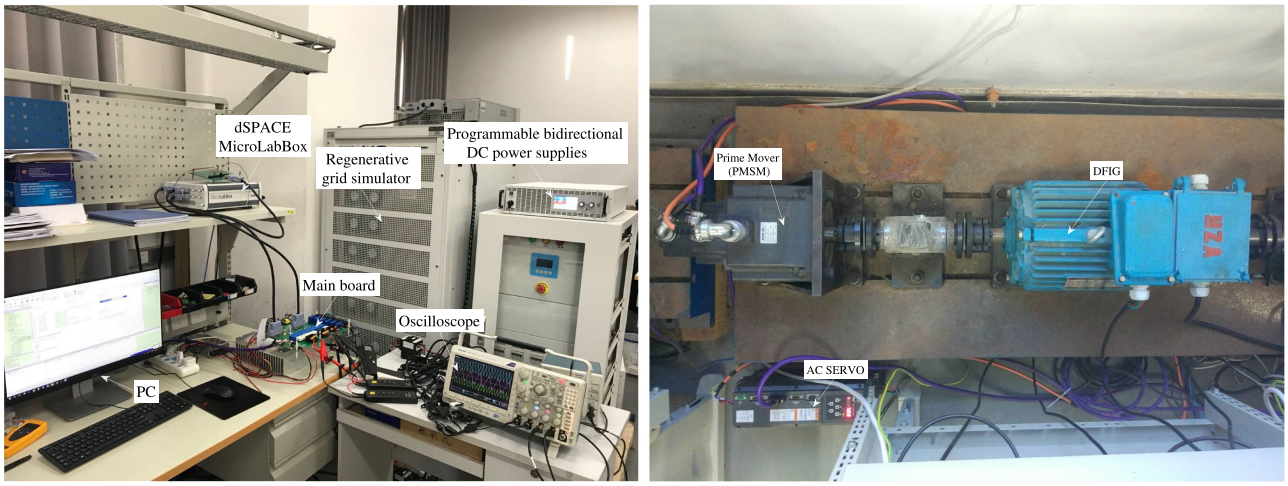

(a) (b)

Fig. 9. Experimental platform for DFIG system. (a) Control and main circuits. (b) DFIG and prime mover.

reference value of the active power is −1000 W, the steady-state error is within ±60 W when the mutual inductance varies from 70% to 130% of its nominal value. Some oscillations are contained in the real value of stator-side active power and extended reactive power when the mutual inductance deviates from its nominal value. This paper focuses on achieving constant stator-side powers and keeping sinusoidal stator currents under unbalanced network conditions. To reduce the influence of the estimated parameter errors, especially the mutual inductance, some online parameter identification methods [30] may be applied to the proposed method for future study.

B. Experimental Results

To confirm the effectiveness of the proposed DPC method in Section III, experimental tests are performed on a two-level DFIG experimental platform. The various parts of the experimental platform are shown in Fig. 9. MicroLabBox from dspace is utilized to implement the control algorithms. The DFIG is driven by a permanent magnet synchronous machine (PMSM), which is fed by an ac servo controller. A bidirectional dc power supply is employed to provide the constant dc bus voltage irrespective of the subsynchronous or supersynchronous operation of the DFIG. During the tests, all the experimental results were recorded using ControlDesk interfaced with MicroLabBox and a PC. These data were further analyzed and plotted using MATLAB.

Fig. 10 shows the steady-state performance of the two DPC-SVM methods under balanced network conditions. From top to bottom, the curves shown in Fig. 10 are the stator-side active power, two types of stator-side reactive power, three-phase stator currents, and three-phase rotor currents. The reference value of the stator-side active power is −1000 W, and the reference value of the reactive power is 0 Var. It is observed that the steady-state performance of the two DPC-SVM methods is almost the same when the grid voltage is balanced. In Fig. 11, the harmonic spectra of the stator current of the two DPC methods are

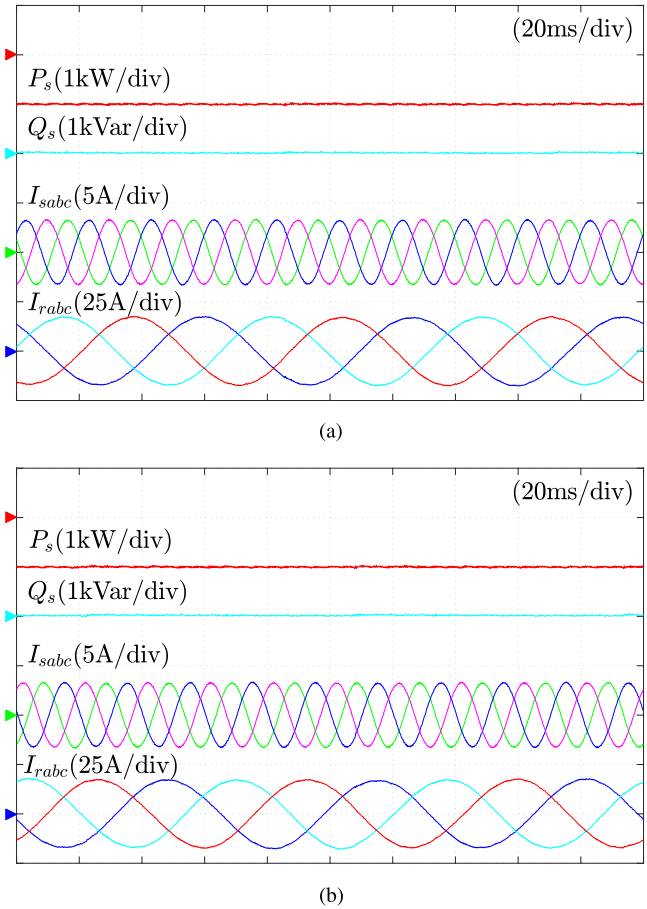

Fig. 10. Steady-state performance of two DPC-SVM methods under balanced network conditions. (a) Conventional DPC-SVM. (b) Proposed DPC-SVM.

presented. In conventional DPC-SVM, the THD of the phase A stator current is 2.14%, and in the proposed DPC-SVM method, the THD of the phase A stator current is 2.12%. The two DPC

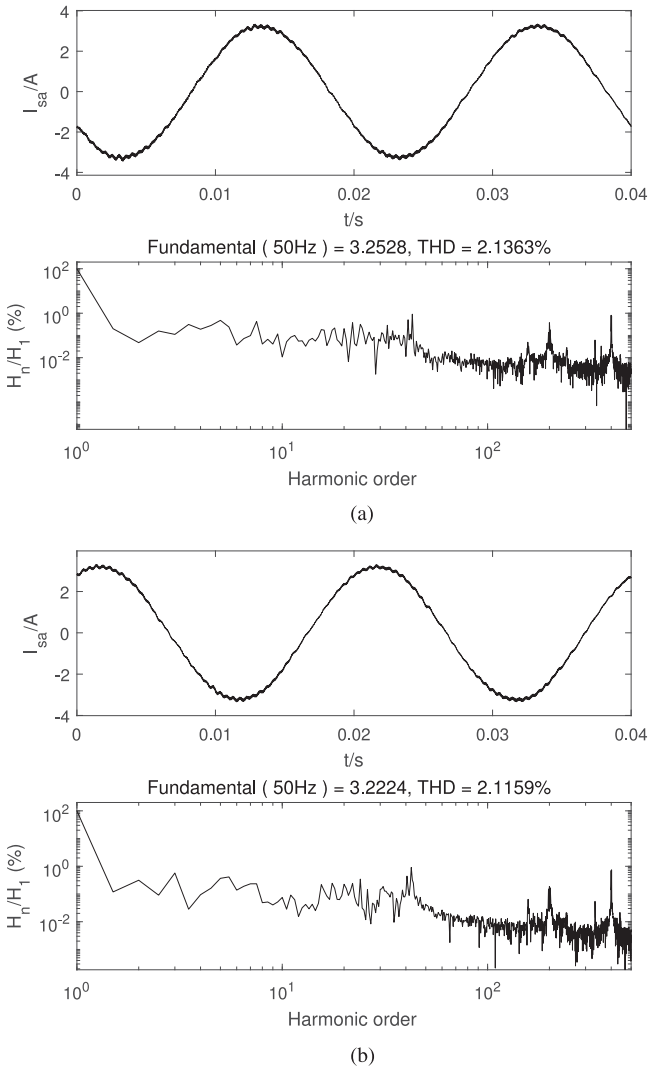

Fig. 11. Harmonic spectra of the stator current under balanced network conditions. (a) Conventional DPC-SVM. (b) Proposed DPC-SVM.

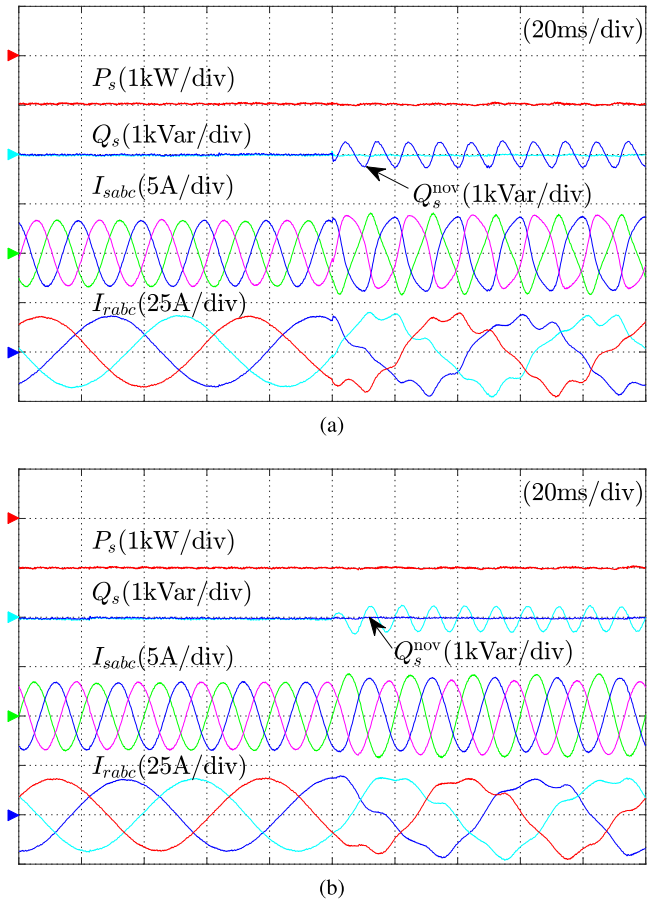

Fig. 12. Experimental results of the two DPC-SVM methods when the network changes from balanced to unbalanced. (a) Conventional DPC-SVM. (b) Proposed DPC-SVM.

methods achieve very similar performances under balanced network conditions, which confirms the previous analysis that the proposed DPC method is equivalent to the conventional DPC method under balanced network conditions.

In Fig. 12, the experimental results of the conventional DPC-SVM and proposed DPC-SVM methods are presented. The phase A grid voltage decreases to 70% of its original value at 0.1 s, which means that the phase A voltage changes from 212 to 148.4 V. After 0.1 s, the conventional reactive power tracks the reference value 0 Var, and the extended reactive power oscillates at twice the network frequency. The stator currents are severely distorted in Fig. 12(a) when the network becomes unbalanced. In Fig. 12(b), after the phase A grid voltage decreases to 70% of its original value in 0.1 s, the extended reactive power closely tracks the reactive reference value without any oscillations. The conventional reactive power oscillates at 100 Hz. The three-phase stator currents are sinusoidal after the grid voltage becomes unbalanced.

The improved steady-state performance of the proposed DPC-SVM can also be confirmed by the harmonic spectra of the phase A stator current of the two DPC-SVM methods. In Fig. 13(a), the THD of the phase A stator current is 11.20% in the conventional DPC-SVM method when the network is unbalanced. In Fig. 13(b), the THD of the phase A stator current is 2.63% under the proposed DPC-SVM method when the grid voltage is unbalanced.

The dynamic responses under the two DPC-SVM methods are investigated in Fig. 14. In Fig. 14(a), the stator active power steps from 0 to -1000 W at 0.1 s, while the stator reactive power remains at 0 Var. In addition, the network remains unbalanced when the phase A grid voltage decreases to 70% of its original value. Similar to Fig. 12(a), the conventional reactive power tracks its reference value without oscillations. In addition, the extended reactive power oscillates at twice the grid frequency: 100 Hz. Fig. 14(b) shows the dynamic responses of the novel DPC-SVM method; after 0.1 s, the three-phase stator currents are sinusoidal. Both the stator-side active power and stator-side extended reactive power track their reference value without oscillations.

Fig. 15 shows the dynamic responses for the two DPC-SVM methods under unbalanced network conditions when the rotor

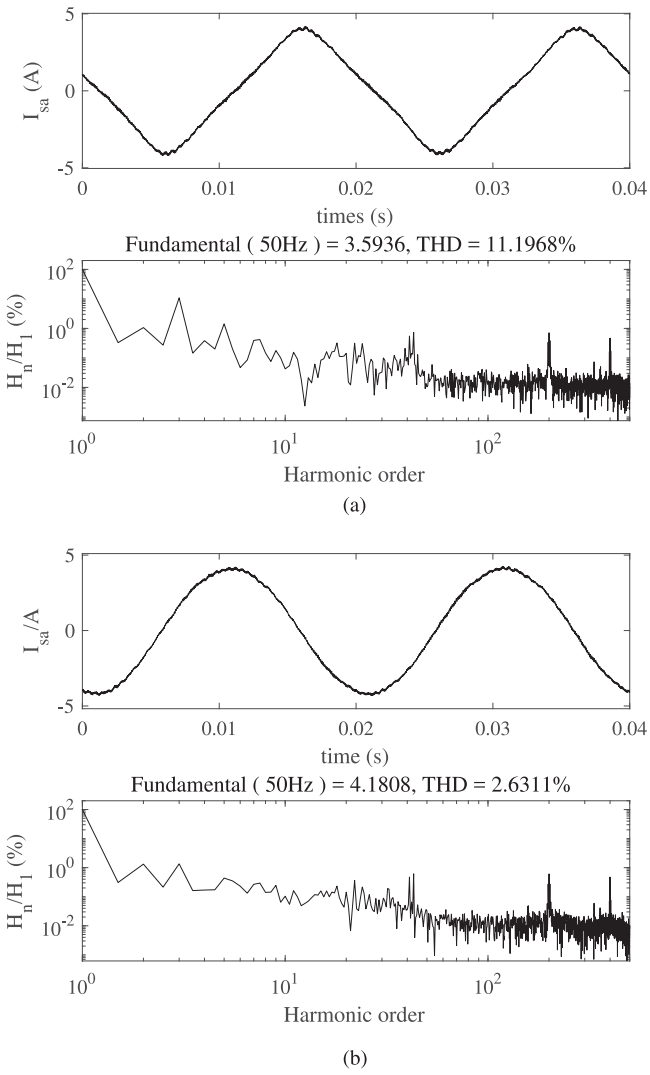

Fig. 13. Harmonic spectra of the stator current when the network is unbalanced. (a) Conventional DPC-SVM. (b) Proposed DPC-SVM.

speed changes from subsynchronous speed to supersynchronous speed. The rotor speed changes from 900 (slip $s = 0.1$) to 1100 r/min (slip $s = -0.1$). In Fig. 15(a), when the rotor speed changes, the real values of the stator-side active power and reactive power track their reference values closely. However, the three-phase stator currents are severely distorted, which confirms that the conventional DPC-SVM method is not appropriate for unbalanced network conditions if no other measure is combined with the DPC method. In contrast, in Fig. 15(b), when the proposed DPC-SVM method is used, the real values of the stator-side active power and extended reactive power follow their reference values closely. Moreover, in the wide speed variation range, the stator currents remain sinusoidal. The control target of simultaneously eliminating the stator-side power ripples and maintaining the sinusoidal stator currents is realized when the DFIG operates at subsynchronous speed and supersynchronous speed.

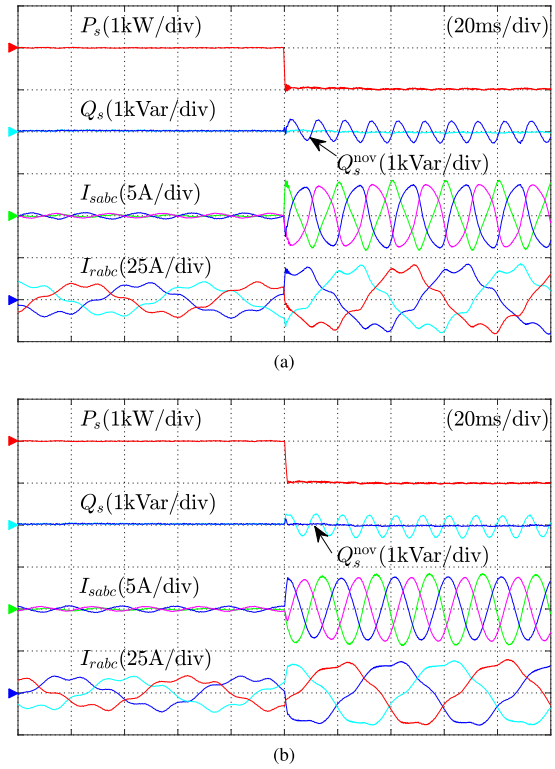

Fig. 14. Dynamic responses of the two DPC-SVM methods to step changes of P_s^{ref} from 0 to -1000 W. (a) Conventional DPC-SVM. (b) Proposed DPC-SVM.

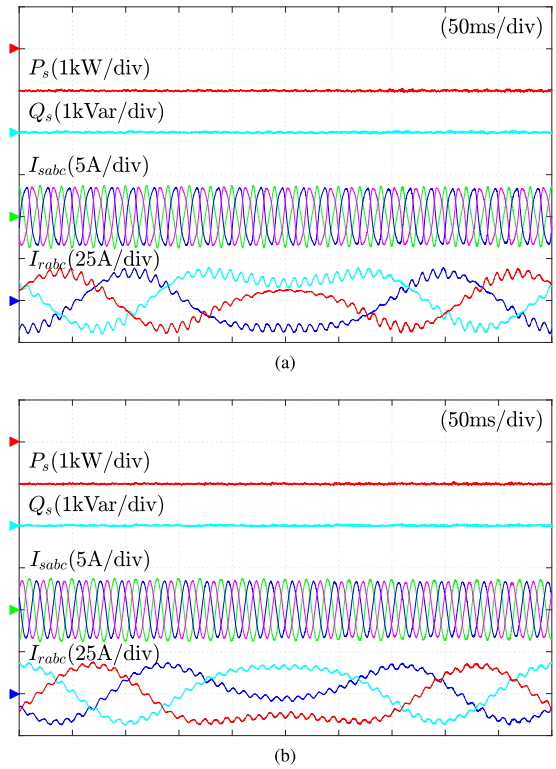

Fig. 15. Dynamic responses of two DPC-SVM methods under unbalanced network conditions when the rotor speed changes from 900 (s = 0.1) to 1100 r/min (s = −0.1). (a) Conventional DPC-SVM. (b) Proposed DPC-SVM.

V. Conclusion

This paper proposes a novel DPC-SVM method for DFIGs that is able to work effectively under both balanced and unbalanced grid voltage conditions. In contrast to the conventional DPC-SVM method, the proposed DPC method adopts extended power theory. The required rotor reference voltage is calculated based on the principle of deadbeat power control. During the calculation process, the power slopes are derived analytically considering the voltage unbalances. Then, SVM is utilized to synthesize the calculated rotor reference voltage. Compared with the state-of-the-art solutions, the proposed DPC-SVM achieves the predefined control target under unbalanced network conditions without any other power compensation terms. The proposed method is compared to conventional DPC-SVM, and its effectiveness is validated by the presented simulation and experimental results under different operating conditions.

References

[1] Z. Chen, J. M. Guerrero, and F. Blaabjerg, "A review of the state of the art of power electronics for wind turbines," *IEEE Trans. Power Electron.*, vol. 24, no. 8, pp. 1859–1875, Aug. 2009.

[2] Y. Zhang, J. Hu, and J. Zhu, "Three-vectors-based predictive direct power control of the doubly fed induction generator for wind energy applications," *IEEE Trans. Power Electron.*, vol. 29, no. 7, pp. 3485–3500, Jul. 2014.

[3] R. Datta and V. Ranganathan, "Direct power control of grid-connected wound rotor induction machine without rotor position sensors," *IEEE Trans. Power Electron.*, vol. 16, no. 3, pp. 390–399, May 2001.

[4] L. Xu and P. Cartwright, "Direct active and reactive power control of DFIG for wind energy generation," *IEEE Trans. Energy Convers.*, vol. 21, no. 3, pp. 750–758, Sep. 2006.

[5] Y. Zhang, Z. Li, Y. Zhang, W. Xie, Z. Piao, and C. Hu, "Performance improvement of direct power control of PWM rectifier with simple calculation," *IEEE Trans. Power Electron.*, vol. 28, no. 7, pp. 3428–3437, Jul. 2013.

[6] H. Zhang, Y. Zhang, and D. Yang, "Two-vectors-based model predictive direct power control of doubly fed induction generator for grid connection and power regulation," *Trans. China Electrotech. Soc.*, vol. 31, no. 5, pp. 69–76, 2016.

[7] Y. Zhang, Z. Li, W. Xu, J. Hu, and J. Zhu, "Grid synchronization of DFIG using model predictive direct power control," in *Proc. Int. Conf. Electr. Mach. Syst.*, Aug. 2011, pp. 1–6.

[8] A. J. S. Filho and E. R. Filho, "Model-based predictive control applied to the doubly-fed induction generator direct power control," *IEEE Trans. Sustain. Energy*, vol. 3, no. 3, pp. 398–406, Jul. 2012.

[9] Y. Zhang, D. Xu, and D. Jiang, "A universal multiple-vectors-based model predictive direct power control for doubly fed induction generators," in *Proc. IEEE Energy Convers. Congr. Expo.*, Oct. 2017, pp. 3337–3344.

[10] Y. Zhang, Y. Bai, and H. Yang, "A universal multiple-vector-based model predictive control of induction motor drives," *IEEE Trans. Power Electron.*, vol. 33, no. 8, pp. 6957–6969, Aug. 2018.

[11] D. Zhi and L. Xu, "Direct power control of DFIG with constant switching frequency and improved transient performance," *IEEE Trans. Energy Convers.*, vol. 22, no. 1, pp. 110–118, Mar. 2007.

[12] Y. Zhang, J. Liu, H. Yang, and J. Gao, "Direct power control of pulsewidth modulated rectifiers without dc voltage oscillations under unbalanced grid conditions," *IEEE Trans. Ind. Electron.*, vol. 65, no. 10, pp. 7900–7910, Oct. 2018.

[13] D. Santos-Martin, J. L. Rodriguez-Amenedo, and S. Arnalte, "Direct power control applied to doubly fed induction generator under unbalanced grid voltage conditions," *IEEE Trans. Power Electron.*, vol. 23, no. 5, pp. 2328–2336, Sep. 2008.

[14] G. Abad, M. A. Rodriguez, G. Iwanski, and J. Poza, "Direct power control of doubly-fed-induction-generator-based wind turbines under unbalanced grid voltage," *IEEE Trans. Power Electron.*, vol. 25, no. 2, pp. 442–452, Feb. 2010.

[15] J. Hu, J. Zhu, and D. G. Dorrell, "Predictive direct power control of doubly fed induction generators under unbalanced grid voltage conditions for power quality improvement," *IEEE Trans. Sustain. Energy*, vol. 6, no. 3, pp. 943–950, Jul. 2015.

[16] C. Cheng, P. Cheng, H. Nian, and D. Sun, "Model predictive stator current control of doubly fed induction generator during network unbalance," *IET Power Electron.*, vol. 11, no. 1, pp. 120–128, 2018.

[17] D. Sun and X. Wang, "Low-complexity model predictive direct power control for DFIG under both balanced and unbalanced grid conditions," *IEEE Trans. Ind. Electron.*, vol. 63, no. 8, pp. 5186–5196, Aug. 2016.

[18] X. Wang and D. Sun, "Three-vector-based low-complexity model predictive direct power control strategy for doubly fed induction generators," *IEEE Trans. Power Electron.*, vol. 32, no. 1, pp. 773–782, Jan. 2017.

[19] D. Sun, X. Wang, H. Nian, and Z. Q. Zhu, "A sliding-mode direct power control strategy for DFIG under both balanced and unbalanced grid conditions using extended active power," *IEEE Trans. Power Electron.*, vol. 33, no. 2, pp. 1313–1322, Feb. 2018.

[20] X. Wang, D. Sun, and Z. Q. Zhu, "Resonant-based backstepping direct power control strategy for DFIG under both balanced and unbalanced grid conditions," *IEEE Trans. Ind. Appl.*, vol. 53, no. 5, pp. 4821–4830, Sep. 2017.

[21] R. V. Jacomini and A. J. S. Filho, "Direct power control strategy to enhance the dynamic behavior of DFIG during voltage sag," in *Proc. 7th Int. Conf. Renew. Energy Res. Appl.*, Oct. 2018, pp. 194–198.

[22] L. Shang and J. Hu, "Sliding-mode-based direct power control of grid-connected wind-turbine-driven doubly fed induction generators under unbalanced grid voltage conditions," *IEEE Trans. Energy Convers.*, vol. 27, no. 2, pp. 362–373, Jun. 2012.

[23] Y. Komatsu and T. Kawabata, "A control method of active power filter where system voltage contains negative-phase-sequence component or zero-phase-sequence component," in *Proc. Int Power Electron. Drive Syst. Conf.*, 1995, pp. 583–586.

[24] Y. Suh and T. A. Lipo, "Modeling and analysis of instantaneous active and reactive power for pwm ac/dc converter under generalized unbalanced network," *IEEE Trans. Power Del.*, vol. 21, no. 3, pp. 1530–1540, Jul. 2006.

[25] Y. Zhang, J. Gao, and C. Qu, "Relationship between two direct power control methods for PWM rectifiers under unbalanced network," *IEEE Trans. Power Electron.*, vol. 32, no. 5, pp. 4084–4094, May 2017.

[26] Y. Zhang and D. Xu, "Direct power control of doubly fed induction generator based on extended power theory under unbalanced grid condition," in *Proc. IEEE 3rd Int. Future Energy Electron. Conf. ECCE Asia*, Jun. 2017, pp. 992–996.

[27] H. Akagi, Y. Kanazawa, and A. Nabae, "Instantaneous reactive power compensators comprising switching devices without energy storage components," *IEEE Trans. Ind. Appl.*, vol. IA-20, no. 3, pp. 625–630, May 1984.

[28] A. V. Timbus, P. Rodriguez, R. Teodorescu, M. Liserre, and F. Blaabjerg, "Control strategies for distributed power generation systems operating on faulty grid," in *Proc. IEEE Int Ind. Electron. Symp.*, 2006, vol. 2, pp. 1601–1607.

[29] P. Rodríguez, A. Luna, R. S. Muñoz-Aguilar, I. Etxeberria-Otadui, R. Teodorescu, and F. Blaabjerg, "A stationary reference frame grid synchronization system for three-phase grid-connected power converters under adverse grid conditions," *IEEE Trans. Power Electron.*, vol. 27, no. 1, pp. 99–112, Jan. 2012.

[30] R. Bhattarai, N. Gurung, S. Ghosh, and S. Kamalasadan, "Parametrically robust dynamic speed estimation based control for doubly fed induction generator," *IEEE Trans. Ind. Appl.*, vol. 54, no. 6, pp. 6529–6542, Nov. 2018.

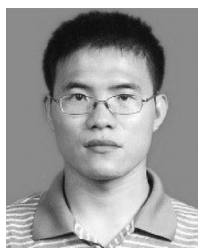

Yongchang Zhang (M'10–SM'18) received the B.S. degree from Chongqing University, Chongqing, China, in 2004, and the Ph.D. degree from Tsinghua University, Beijing, China, in 2009, both in electrical engineering.

From August 2009 to August 2011, he was a Postdoctoral Fellow with the University of Technology Sydney, Ultimo, NSW, Australia. He joined the North China University of Technology in August 2011 as an Associate Professor. He is currently a Full Professor and the Director of Inverter Technologies Engineering Research Center of Beijing, Beijing, China. He has published more than 100 technical papers in the area of motor drives, pulsewidth modulation, and ac–dc converters. His current research interest includes model predictive control for power converters and motor drives.

Jian Jiao was born in 1993. He received the B.S. degree in electrical engineering from Shijiazhuang Tiedao University, Hebei, China, in 2015. He is currently working toward the M.S. degree in electrical engineering in the North China University of Technology, Beijing, China.

His current research interests include predictive control of doubly fed induction generators and pulsewidth modulation rectifiers.

Donglin Xu was born in 1992. He received the B.S. degree in electrical engineering from the North China University of Technology, Beijing, China, in 2015, where he is currently working toward the master's degree in electrical engineering.

His research interests include model predictive control of doubly fed induction generators.